PERFORMANCES OF LPT AND LINEAR CASCADES AT LOW REYNOLDS NUMBERS

A.D. Nepomnyashchiy*, I.V. Tsvetkov*, S.V. Suntsov*, S.Y. Danilkin*
***Central Institute of Aviation Motors (CIAM)**

Keywords: *turbine's model stage, linear cascade, Reynolds number, turbulence*

Abstract

The paper presents some results of a low pressure turbine's model stage (MS) experimental investigation at the Reynolds numbers in the range of $1.3 \cdot 10^5 – 0.13 \cdot 10^5$ at different values of inlet flow's turbulent parameters. Flow's turbulent parameters at the MS's inlet were measured by means of the fast-response pressure probe.

Some results of experimental investigations of the linear cascades to have been the models and modified models of the investigated MS's vanes and blades are also presented. The investigations of the linear cascades were performed at the Reynolds numbers in the range of $5.0 \cdot 10^5 – 0.5 \cdot 10^5$.

1 Introduction

The development of the high efficiency low pressure turbine (LPT) operating at low Reynolds numbers is a challenge for further investigations.

The assessment of turbofan engines LPT's efficiency drop could be about 2% from the sea level up to the altitude of cruise flight [1]. What would be the LPT's efficiency drop for much lower Reynolds numbers? Some results could be observed in [2], [3], [4].

The paper [2] concerns the experimental data of BR715 LPT obtained on a test rig at various Reynolds numbers. The LPT was investigated with the differences in a blades' load. The overall LPT's efficiency drop from the sea level up to the ~ 13.5 km (average blade rows Reynolds number is about $0.85 \cdot 10^5$) was ~ 1.5%.

The results of PW 545 LPT's efficiency experimental assessment could be seen in [3]. The LPT's investigations were carried out as a part of an engine and performed both on an engine's test rig and in a flight test. The investigations were fulfilled in the range of Reynolds numbers $3.0 \cdot 10^5 – 0.3 \cdot 10^5$. The measured LPT's efficiency drop was ~ 7%.

In mentioned conditions probably there was a lack of torques' data of an engine's shafts. In that case the estimation of LPT's efficiency operated as a part of an engine is performed through the integration of all engine's systems (fan, compressor, combustion chamber, high pressure turbine, LPT).

The wider range of Reynolds numbers to investigate the LPT on a test rig can be seen in [4]. The investigated LPT was a three turbine's stages. The LPT was tested in the range of Reynolds numbers (an arithmetic average of the chord and exit velocity based Reynolds number of six airfoils) $5.2 \cdot 10^5 – 0.4 \cdot 10^5$. The estimated LPT's efficiency drop was ~ 6%.

This paper presents some results of the MS experimental investigation at the Reynolds numbers in the range of $1.3 \cdot 10^5 – 0.13 \cdot 10^5$. The MS's investigation was conducted at two different values of inlet flow's turbulent parameters.

There are lots of investigations' results of linear turbine's cascades at low Reynolds numbers in the literature, see as example [5], [6], [7]. The main objective of these investigations is to obtain the better geometrics of airfoils ensured minimum losses of a flow's kinetic energy.

This paper also presents some results of experimental investigations of two groups of stationary linear cascades at the Reynolds numbers in the range of $5.0 \cdot 10^5 – 0.5 \cdot 10^5$. The both groups consist of two cascades. The first group cascades were designed to have been the

models of the investigated MS's vanes and blades on the middle diameter. The second group cascades were designed to have been the modified models of the MS's vanes and blades on the middle diameter. The blades geometry within the first group corresponds to the aft loaded distribution. The blades geometry within the second group corresponds to the front loaded distribution.

2 Experimental Objects

2.1 The MS's Experimental Module

The scheme of the experimental module to investigate of the MS on a test rig is shown on Fig. 1.

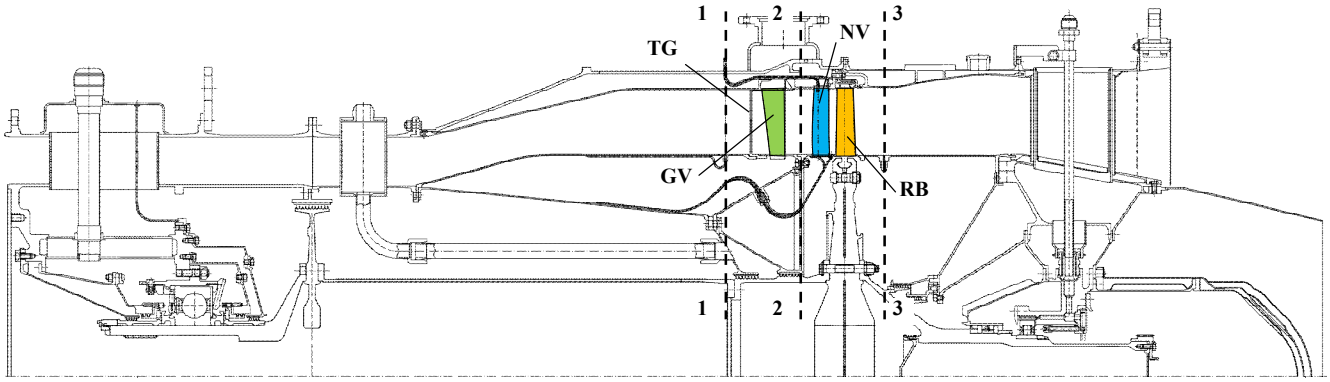

Fig. 1. The scheme of the experimental module to investigate of the MS on a test rig.

The MS consists of the guide vanes (GV), the nozzle vanes (NV) and the rotor blades (RB) as it's shown on Fig. 1. The experimental investigations of the MS were conducted with and without of the turbulizing grid (TG).

The MS's experimental investigations were carried out on pure heated up to the total temperature of $T_0^* = 450 – 550$ K air flow at the Reynolds numbers (an arithmetic average of the chord and the exit velocity based Reynolds numbers of the NV and the RB of the MS) in the range of $1.3 \cdot 10^5 – 0.13 \cdot 10^5$. The lower Reynolds numbers had been gained by varying the total pressure p_0^* of a flow at the MS's inlet in the range of 0.9 – 0.075 bar. The total-to-total pressure ratio of a flow in the MS was $\pi^* = 1.7$. The speed ratio of the MS was $u/c_{is} = 0.48$ (the equivalent loading factor is $h/u^2 = 2.17$).

2.2 The Linear Cascades

The profiles' geometrical parameters of the investigated linear cascades are shown in the Table 1. The scheme and parameters of the experimental rig to investigate linear cascades as well as the main parameters of linear cascades are presented in [7].

The cascades #1 and #2 were designed to have been the models of the investigated MS's vanes (#1) and blades (#2) on the middle diameter and have the aft loaded distribution. The results of the cascade #2 investigations are presented in [7].

The cascades #3 and #4 were designed based on the cascades #1 and #2 to have maintained the main parameters such as the blades' pitches, the blades' chords, the blades' angles, the diameters of leading and trailing edges without changes (see Table 1) but to have made the front loaded distribution. The loading level in cascades is characterized by the static pressure distribution over the blades' surface [5].

Table 1 Geometrical parameters of the linear cascades

	$\beta_{1c.}$	$\beta_{2eff.}$	$\bar{C}_m$	$\bar{t}$	δ	$\bar{d}_1$	$\bar{d}_2$	γ
1	52.4	25.1	0.144	0.793	18.1	0.049	0.039	40.6
2	48.8	33.5	0.128	0.710	21.3	0.031	0.035	23.4
3	52.4	25.1	0.112	0.793	9.46	0.049	0.039	47.8
4	48.8	33.5	0.114	0.710	10.1	0.031	0.035	32.4

where

$\beta_{1c.}$ – the designed inlet angle of the blade in the cascade, degree;

$\beta_{2eff.}$ – the effective outlet angle calculated as the *arcsine* of the ratio between the cascade's throat to the cascade's blades pitch, degree;
$\overline{C}_m$ – the ratio between the profile's maximum thickness to the blade's chord;
$\bar{t}$ – the non-dimensional pitch defined as the ratio between the cascade's blades pitch to the blade's chord;
δ – the unguided turning angle, degree [5];
$\overline{d}_1$ – the ratio between the leading edge's diameter to the blade's chord;
$\overline{d}_2$ – the ratio between the trailing edge's diameter to the cascade's throat;
γ – the stagger angle, degree [5].

As can be noticed in the Table 1, the unguided turning angles of the aft loaded cascades are higher compared to ones of the front loaded cascades and inversely for the stagger angles.

The blades' shapes of cascades #1 - #4 are plotted on the Fig. 2.

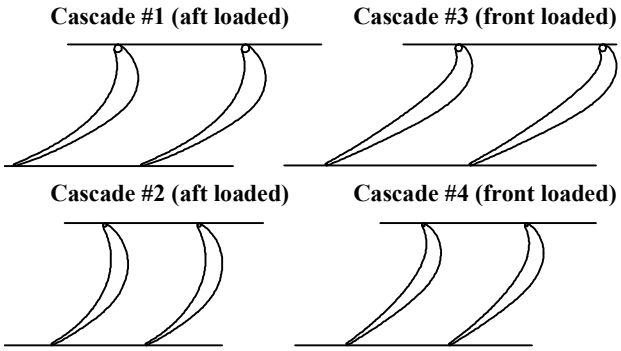

Fig. 2. The blades' shapes of the cascades #1 - #4.

The cascades were investigated on the test rig located in the CIAM. The investigations were conducted at the Reynolds numbers (based on the blade's chord and the isentropic flow's velocity at the cascade's outlet) in the range of $5.0 \cdot 10^5 – 0.5 \cdot 10^5$. The variation of the Reynolds number was attained by changing the flow's total pressure at the cascades' inlet p_0^* in the range of 0.2 – 0.8 bar and isentropic flow's velocity at the cascades' outlet λ_{is}, see equation (9), in the range of 0.3 – 0.85.

The investigations were performed with and without using the turbulizung grid located in front of the cascades [7]. The turbulizing grid was designed by the recommendations [8].

At the higher Reynolds number the turbulence intensity of the streamwise velocity fluctuation in front of the cascades was ~ 0.04 and ~ 0.15 without and with the turbulizing grid, respectively (measured by means of the fast-response pressure probe Kulite-FAP-HT-250) [7]. As the Reynolds number decreases the turbulence intensity increases [7].

3 Instrumentations

3.1 The MS's Instrumentations

The MS was investigated on the test rig located in the CIAM.

The MS's power was absorbed by the hydraulic brake. The maximum MS's power was 750 kW (at the inlet flow's total pressure of $p_0^* = 0.9$ bar); the minimum MS's power was 30 kW (at the inlet flow's total pressure of $p_0^* = 0.075$ bar). The hydraulic brake had been calibrated before the experimental investigations were conducted.

The air flow at the MS's inlet was measured by means of the orifice plate. To avoid the influence of low Reynolds numbers on the orifice plate's meterage the air pipeline route had been designed to have ensured the flow's total pressure at the orifice plate's inlet not less than $p_0^* = 2$ bar at the all MS's operating modes.

To have gained flow's total pressure at the MS's inlet in the range of $p_0^* = 0.9 – 0.07$ bar the throttle had been mounted inside the pipeline route behind the orifice plate. The experimental rig was operated on the excess pressure mode at the inflow collector and on the exhauster pressure mode at the outflow collector. As an example, the flow's total pressure of $p_0^* = 0.075$ bar at the MS's inlet had been attained at the flow's total pressure of $p_0^* = 2$ bar at the orifice plate's inlet.

Moreover the orifice plate had been calibrated by means of the etalon critical nozzle at the inlet flow's total pressure of $p_0^* > 2$ bar and at the mass flow having corresponded to the MS's mass flow before the experimental investigations were performed.

The experimental rig had been checked on the absence of leakages of the atmospheric air into the air route from the orifice plate's inlet up to the experimental module's outlet. The checking had been done by vacuumizing the

whole air route up to the pressure of 0.4 bar. The pressure probes located in a various parts of the experimental module and the pipeline had shown the same value of 0.4 bar.

At the MS's inlet in the section 1-1, see Fig. 1, the total pressure was measured by means of three rakes at five points along the radius of a flow part; the total temperature was measured by means of three rakes of thermocouples at five points along the radius. The static pressure in the section 1-1 was measured at the hub and at the shroud of a flow part at four points around the circumference.

Turbulent flow's parameters were measured by means of fast-response pressure probe Kulite FAP-HT-250 [9], [10] in the section 2-2 of a flow part, see Fig. 1.

On the leading edges of the three blades of the NV, see Fig. 1, the total pressure was measured by means of the Pitot tubes at five points along the radius. At the NV's outlet the static pressure was measured at the hub and at the shroud of a flow part at four points around the circumference.

At the MS's outlet in the section 3-3, see Fig. 1, the total pressure was measured by means of three rakes at seven points along the radius of a flow part; the total temperature was measured by means of three rakes of thermocouples at five points along the radius.

In addition, the flow's pitch angles (the flow's angles in the circumferential direction) were measured by means of three rakes at nine points along the radius of a flow part. The each rake had the three points along the radius of a flow part but radii of points were different for all rakes.

The pressure was also measured in the MS's cavities.

The measurement errors were as follows: for the pressure - 0.1%, for the temperature - 0.2%, for the torque - 0.5%, for the rotor speed - 0.1%, for the mass flow of the air at the MS's inlet - 0.5%.

The error in evaluations of the MS's efficiency at the Reynolds number of $Re = 1.3 \cdot 10^5$ was 1%; at the Reynolds number of $Re = 0.13 \cdot 10^5$ was 4%.

3.2 The Linear Cascades' Instrumentations

The linear cascades' instrumentation, measurements location and the technique of data's acquisition are presented in [7].

The error of the pressure acquisition for each measuring channel wasn't higher than 0.15%.

3.3 The Fast-Response Probe Calibration at Low Reynolds Numbers

The turbulence measurements in a flow part of the MS were conducted at the low Reynolds numbers by means of the fast-response pressure probe Kulite FAP-HT-250.

The fast-response pressure probe had been calibrated in the calibration nozzle in the range of Reynolds numbers of $Re = 6 \cdot 10^4 - 1 \cdot 10^4$ (based on the flow's velocity and the characteristic size of 10 mm) before it was used in the experimental investigation of the MS.

The mentioned variation of the Reynolds number was attained by the changing of the flow's total pressure in the range of $p_0^* = 0.8 - 0.2$ bar and the flow's reduced velocity in a range of $\lambda = 0.65 - 0.3$.

Here and below the reduced velocity λ is calculated as the ratio between the flow velocity and the critical velocity of a sound a_{cr}. The critical velocity of a sound is calculated by following equation:

$$a_{cr} = \sqrt{\frac{2 \cdot k}{k+1} \cdot R \cdot T_0^*} \qquad (1)$$

where

T_0^* – the total temperature of the flow;

R – the gas constant of the air.

The data obtained by means of the fast-response pressure probe in the calibration nozzle were compared with the data obtained by means of the hot-wire probe DANTEC CTA 56C17 at the same conditions.

The turbulence measurement having performed by means of hot-wire probe was done at the same range of the flow's total pressure as for the fast-response pressure probe but in the range of the flow's reduced velocity of $\lambda = 0.1 - 0.3$.

The turbulence intensity of the streamwise velocity fluctuation versus the Reynolds number is shown on Fig. 3.

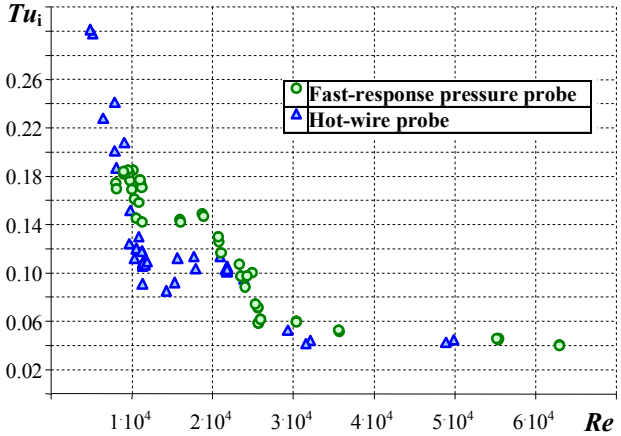

Fig. 3. The turbulence intensity of the streamwise velocity fluctuation in the calibration nozzle.

As it's shown on the Fig. 3, there is a good coincidence between the data of the fast-response pressure probe and the hot-wire probe.

The growth of turbulence intensity at the Reynolds numbers $Re < 3.10^4$, see the Fig. 3, could be explained by influence of the honeycomb located in the calibration nozzle at the distance of ~ 380 mm upstream the measurement location.

4 Results and Discussion

4.1 The Results of the MS's Experimental Investigations

The MS's normalized efficiency versus the Reynolds number at the operation's mode with the constant value of the total-to-total pressure ratio of $\pi^* = 1.7$ and with the constant value of the stage's speed ratio of $u/c_{is} = 0.48$ are shown on Fig. 4.

The MS's characteristics depicted on the Fig. 4 corresponding to the experimental data obtained with and without the TG located upstream from the NV, see Fig. 1, were normalized by the base value of the MS's efficiency at the Reynolds number of $Re = 1.3 \cdot 10^5$ obtained without the TG.

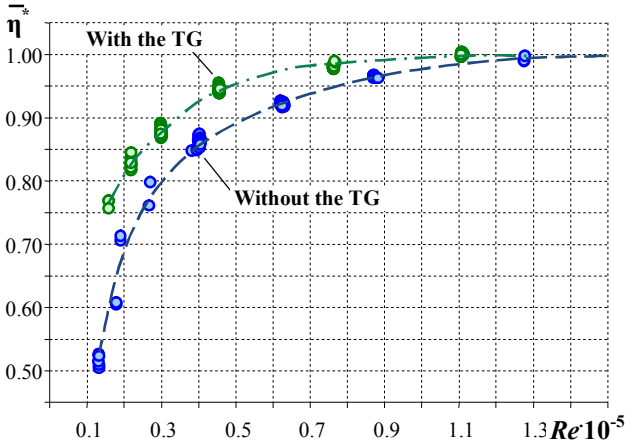

Fig. 4. The MS's normalized efficiency versus the Reynolds number.

The MS's efficiency is calculated using the following formula:

$$\eta^* = \frac{N}{G_0 \cdot H_0^*} \qquad (2)$$

where

N - the MS's power measured by the hydraulic brake;

G_0 - the air's mass flow measured by means of the calibrated orifice plate;

H_0^* - the isentropic MS's total-to-total heat drop,

$$H_0^* = \frac{k}{k-1} \cdot R \cdot T_0^* \cdot (1 - \pi^{*\frac{1-k}{k}}) \qquad (3)$$

As it's seen from the Fig. 4, the efficiency drop of a turbine's stage could be huge at the Reynolds numbers in the range of $Re < 0.6 \cdot 10^5$. Moreover the turbine stage's efficiency depends on the flow's turbulent parameters at its inlet.

As it's seen on the Fig. 4, the MS's efficiency dependencies versus the Reynolds number are nonlinear.

The turbulence intensity and the integral length scale [8] of the streamwise velocity fluctuation measured by means of the fast-response pressure probe in front of the NV (the section 2-2, the Fig. 1) during the MS's investigation versus the Reynolds number are plotted on the Fig. 5 and Fig. 6. The Reynolds number is calculated using the flow velocity measured by the fast-response pressure probe and the characteristic size of 10 mm.

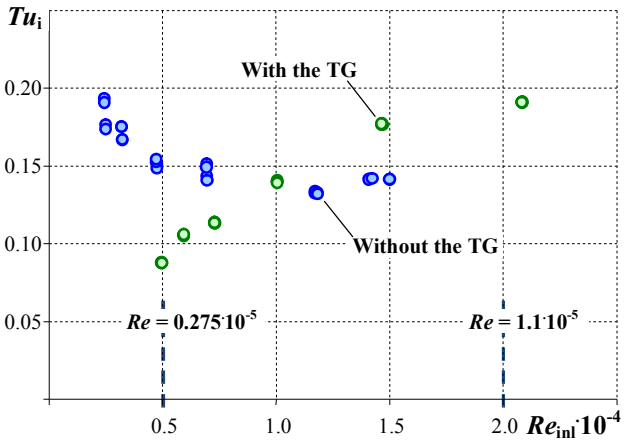

Fig. 5. The turbulence intensity of the streamwise velocity fluctuation in front of the NV.

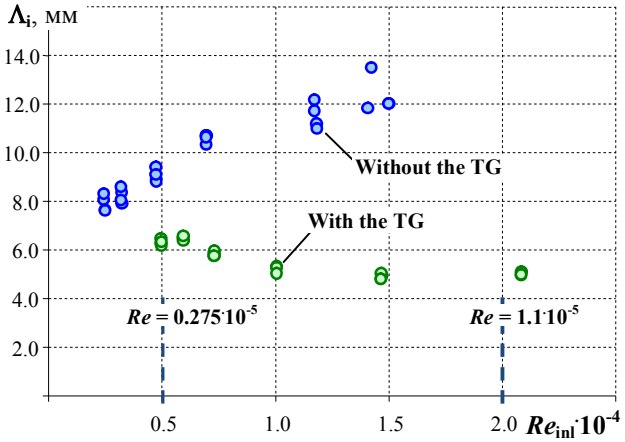

Fig. 6. The integral length scale of the streamwise velocity fluctuation in front of the NV.

The integral length scale depicted on the Fig. 6 was obtained from the turbulent power spectrum of the streamwise velocity fluctuation having used the Taylor hypothesis [11] and having assumed that autocorrelation function has the exponential law [11].

It's seen form the Fig. 4 – 6 that the higher level of the turbulence intensity of the streamwise velocity fluctuation and the lower level of the integral length scale have led to the deceleration of the MS's efficiency drop at low Reynolds numbers. This is probably occurred due to the decreasing of flow separations' intensity on the blades' suction sides that have led to the losses reducing.

As could be noticed from the Fig. 4, if the MS's characteristic obtained without the TG was shifted to the lower value of Reynolds numbers the both characteristics would coincide.

The turbine stage's efficiency change with the Reynolds number could occur not only due to the growth of flow separations' intensity on the blades' suction sides but due to the change in the turbine stage's operation mode.

The MS's reaction ratio versus the Reynolds number is shown on Fig. 7. The turbine stage's reaction ratio is defined using the following equation:

$$\rho = 1 - \frac{H_{NV}}{H_{Stage}} \qquad (4)$$

where

ρ - the turbine stage's reaction ratio;

H_{NG} - the isentropic total-to-static heat drop in the NV,

$$H_{NV} = \frac{k}{k-1} \cdot R \cdot T_0^* \cdot (1 - \pi_{NV}^{\frac{1-k}{k}}) \qquad (5)$$

π_{NV} - the total-to-static pressure ratio in the NV;

H_{Stage} - the isentropic total-to-static heat drop in the MS,

$$H_{Stage} = \frac{k}{k-1} \cdot R \cdot T_0^* \cdot (1 - \pi_{Stage}^{\frac{1-k}{k}}) \qquad (6)$$

π_{Stage} - the total-to-static pressure ratio in the MS (in the turbine stage).

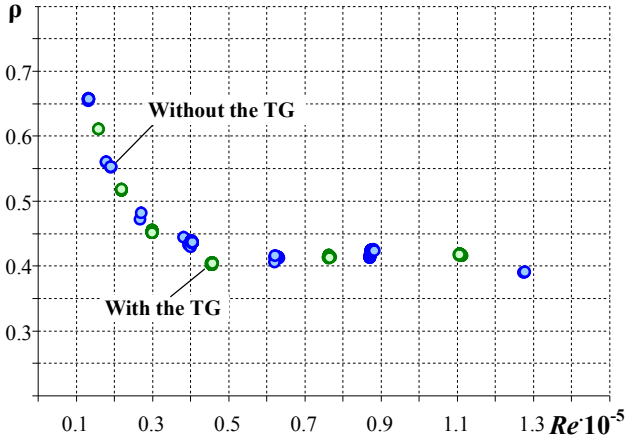

Fig. 7. The MS's reaction ratio versus the Reynolds number.

The MS's reaction ratio rises as the Reynolds number reduces, see the Fig. 7. This means that at lower Reynolds numbers the RB operates with the incidence of the flow's angle towards the blades' suction sides and with the higher flow's outlet velocity in the relative motion.

The reaction ratio could rise due to the reduction of the flow's angle in the

circumferential direction at the NV's outlet and due to the decrease in the flow capacity of the RB at low Reynolds numbers.

4.2 The Results of the Linear Cascades' Experimental Investigations

The profile losses in the linear cascades #1 - #4 (see Table 1) versus the Reynolds number calculated using the blade's chord and isentropic flow's velocity, see the equation (9), at the cascades' outlet are shown on Fig. 8 - 11.

The profile losses are the losses of the flow's kinetic energy, see the equation (8), in the linear cascades outside the zones of secondary flows appearing nearby the end walls. The profile losses are calculated using the measured at the blades' mid height averaged total pressures at the cascade's inlet p_0^* and outlet p_2^* and the averaged pressure at the cascade's outlet p_2 as follows:

$$\lambda_2 = \sqrt{\frac{k+1}{k-1}\cdot\left(1-\left[\frac{p_2}{p_2^*}\right]^{\frac{k-1}{k}}\right)} \qquad (7)$$

$$\zeta_{pr.} = 1-\left(\frac{\lambda_2}{\lambda_{is}}\right)^2 \qquad (8)$$

where

p_2^* - the averaged total pressure at the cascade's outlet;

λ_2 - the averaged reduced velocity at the cascade's outlet;

λ_{is} - the operating mode (the isentropic reduced flow's velocity at the cascade's outlet),

$$\lambda_{is} = \sqrt{\frac{k+1}{k-1}\cdot\left(1-\left[\frac{p_2}{p_0^*}\right]^{\frac{k-1}{k}}\right)} \qquad (9)$$

$\zeta_{pr.}$ - the profile losses.

As it's seen on the Fig. 8 – 11, the front loaded linear cascades shows the higher losses' sensitivity to the low Reynolds numbers compared to the aft loaded linear cascades. The profile losses in the aft loaded cascades #1, #2 are lower than in the front loaded cascades #3, #4 respectively at low Reynolds numbers.

The experimental investigation has shown that the profile losses in the linear cascade #1 depend on inlet flow's turbulent parameters at low Reynolds numbers, see the Fig. 8. The slight dependence of the profile losses on inlet flow's turbulent parameters at low Reynolds numbers observes in the linear cascade #2, see the Fig. 9.

As mentioned above the linear cascades #1 and #2 are the models of the MS's vanes and blades on the middle diameter respectively. Probably that's why the same result of impact of the inlet flow's turbulent parameters on the MS's efficiency was achieved, see the Fig. 4.

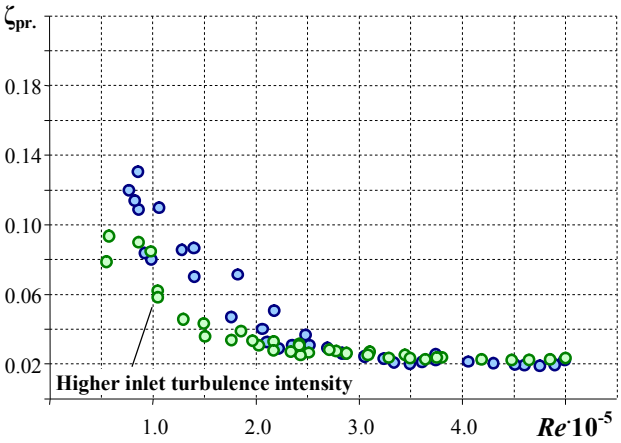

Fig. 8. The profile losses versus the Reynolds number in the linear cascade #1.

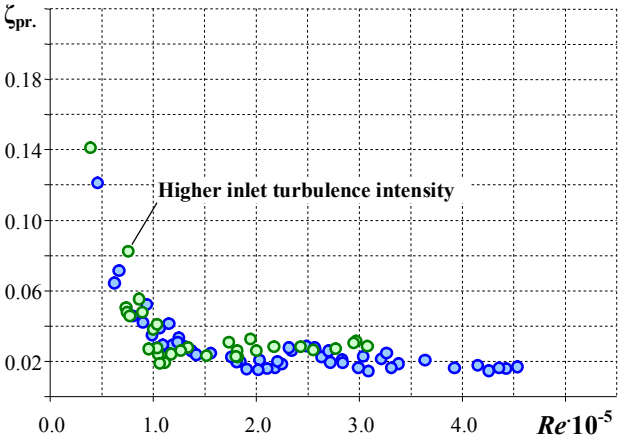

Fig. 9. The profile losses versus the Reynolds number in the linear cascade #2.

The absence of influence of inlet flow's turbulent parameters on the profile losses at low Reynolds numbers are observed in the front loaded linear cascades #3 and #4, see the Fig. 10 - 11. The higher turbulence intensity has led towards the growth of the profile losses in

the linear cascade #4 at higher Reynolds numbers, see the Fig. 11.

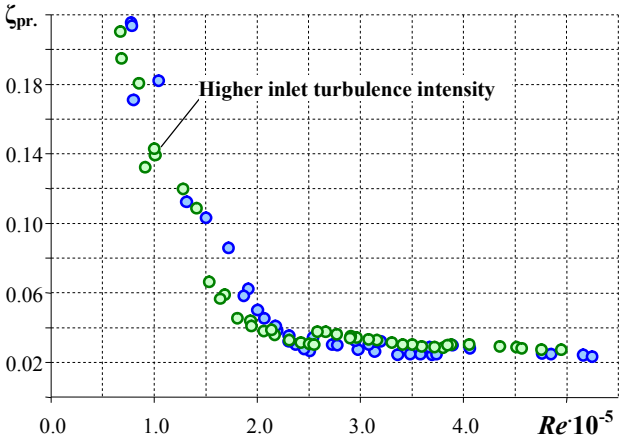

Fig. 10. The profile losses versus the Reynolds number in the linear cascade #3.

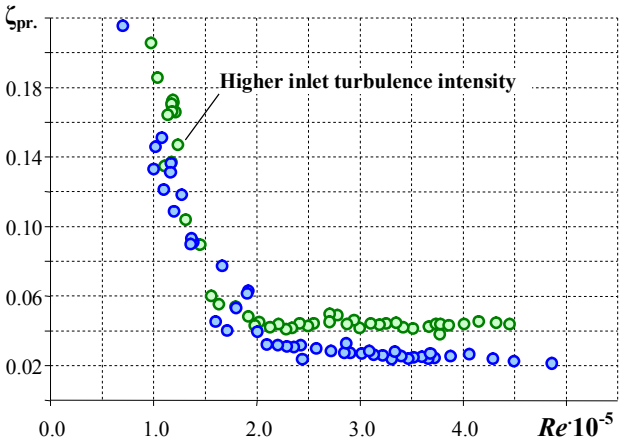

Fig. 11. The profile losses versus the Reynolds number in the linear cascade #4.

Possibly the front loaded profiles could be applied in vanes and blades of the LPT after carrying out more complex redesign of their blades' channels to gain the lower profile losses at low Reynolds numbers.

The data acquired in the experimental investigations of the linear cascades #1 - #4 were complemented to data of experimental investigations of other cascades to get more comprehensive estimation of the Reynolds number influence on the profile losses.

There was an attempt to generalize the influence of low Reynolds numbers on the profile losses in linear cascades. The generalization has shown that the losses' growth in linear cascades could be approximately defined as the power function as follows $\zeta/\zeta_0 = (Re/Re_0)^{-0.88}$ [12]. Where Re_0 – the Boundary Reynolds number, the Reynolds number of the boundary of the self-similarity region of a flow; ζ_0 – the profile losses in the self-similarity region of a flow.

Investigations have shown that the Boundary Reynolds number is a function of blades' geometry and inlet flow's turbulent parameters. In this case the problem of achieving the lower profile losses in vanes and blades of the LPT at low Reynolds numbers could be solved by minimizing the Boundary Reynolds number via finding the blades' optimal geometrical parameters.

5 Conclusion

The MS was experimentally investigated on the turbine's test rig at low Reynolds numbers in the range of $Re = 1.3 \cdot 10^5 - 0.13 \cdot 10^5$ at different values of inlet flow's turbulent parameters.

The two groups of the stationary linear cascades were experimentally investigated on the exhauster rig at low Reynolds numbers in the range of $Re = 5.0 \cdot 10^5 - 0.5 \cdot 10^5$ at different values of inlet flow's turbulent parameters. The first group of cascades was designed to have been the models of the investigated MS's vanes and blades on the middle diameter. The second group cascades were designed to have been the modified models of the MS's vanes and blades on the middle diameter. The blades geometry within the first group corresponds to the aft loaded distribution. The blades geometry within the second group corresponds to the front loaded distribution.

The investigations have shown the following:

- The efficiency drop in a turbine's stage could be huge at the Reynolds numbers in the range of $Re < 0.6 \cdot 10^5$.
- The specific inlet flow's turbulent parameters could lead to deceleration of a turbine stage's efficiency drop at low Reynolds numbers.
- The turbine's stage efficiency dependency on the Reynolds number is nonlinear. In this case the Reynolds number calculated as averaged Reynolds numbers of each blades of a multistage LPT to be used as a parameter for an

estimation of its efficiency drop isn't correct.

- The profile losses in the front loaded cascades are less sensitive to inlet flow's turbulent parameters at low Reynolds numbers as compared to the aft loaded cascades. The efficiency of a turbine's stage designed using aft loaded profiles probably is more sensitive to inlet flow's turbulent parameters.
- Turbulence measurements in a flow part of turbines shows that the turbulence intensity could raise up to values of 15% - 20%, see, as example, [13], [14]. The profile losses in aft loaded cascades at low Reynolds numbers decrease as the inlet flow's turbulent intensity increases. That could be a cause of using aft loaded profiles in vanes and blades of a LPT.
- Results of conducted investigations could be used to develop a way of blades geometry design combining merits of aft loaded and front loaded distributions.

References

[1] Asphis D. The NASA Low-Pressure Turbine Flow Physics Program. *Minnowbrook II 1997 Workshop on Boundary Layer Transition in Turbomachines*, *Conference publication,* NASA CP – 1998-206958, 1998.

[2] Haselbach F., Schiffer H.-P., Horsman M., Dressen S., Harvey N., Read S. The Application of Ultra High Lift Blading in the BR715 LP Turbine. *ASME Journal Turbomachinery*, Vol. 124, pp. 45-51, 2002.

[3] Castner R., Chiappetta S., Wyzykowski J., Adamczyk J. An Engine Research Program Focused on Low Pressure Turbine Aerodynamic Performance. *ASME Paper*, GT2002-30004, 2002.

[4] Hura H.S., Joseph J., Halstead D.E. Reynolds Number Effect in a Low Pressure Turbine. *ASME Paper*, GT2012-68501, 2012.

[5] Parkash C., Cherry D.G., Shin H.W., Machnaim J., Dialey L., Beacock R., Halstead D., Wadia A.R., Guillot S., Ng W.F., 2008, "Effect of Loading Level and Distribution on LPT Losses". *ASME Paper*, GT2008-50052, 2008.

[6] Hoheisel H., Kiock R., Lichtfuss H.J., Fottner L. Influence of Free-Stream Turbulence and Blade Pressure Gradient on Boundary Layer and Loss Behavior of Turbine Cascades. *ASME Journal of Turbomachinery*, Vol. 109, No. 2, pp. 210-219, 1987.

[7] Nepomnyashchiy A.D., Suntsov S.V., Danilkin S.Y., Maslov V.P. Effect of Reynolds Number, Operating Mode, Turbulence Parameters on Profile and Secondary Losses of LPT. *ICAS paper*, ICAS2016-7.5.2-2016_0276, 2016.

[8] Roach P.E. The generation of nearly isotropic turbulence by means of grids. *Int. J. Heat Fluid Flow*, 8(2), 82-92, 1987.

[9] Flow angle probe high temperature miniature is pressure transducer FAP-HT-250 series. URL: http://www.kulite.com/docs/products/FAP-HT-250.pdf.

[10] Nepomnyashchiy A.D. Turbulence Measurements in a Flow Part of Turbomachines Using a High-Frequency Pressure Probe. *ICAS paper*, ICAS2014-7.4.3-2014_0252, 2014.

[11] Hinze J.O. *Turbulence.* 1st edition, McGraw-Hill, 1959.

[12] Nepomnyashchiy A.D. Generalization of Experimental Data of Flat Turbine Cascades Purging. *Pumps. Turbines. Systems*, № 4(21), 2016.

[13] Zaccaria M., Lakshminarayana B. An Experimental Investigation of Steady and Unsteady Flow Field in an Axial Flow Turbine. *Contractor Report*, NASA CR-4778, 1997.

[14] Göttlich E., Marn A., Pecnik R., Malzacher F.J., Schennach O., Pirker H.P. The Influence of Blade Tip Gap Variation on the Flow Through an Aggressive S-Shaped Intermediate Turbine Duct Downstream a Transonic Turbine Stage - Part II: Time-Resolved Results and Surface Flow. *ASME Paper*, GT2007-28069, 2007.

Copyright Statement

Contact Author Email Address

Mail to: nepomnashi@ciam.ru
nepomnashi@gmail.com